



**HAL**  
open science

# Lubricant Depletion-Resistant Slippery Liquid-Infused Porous Surfaces via Capillary Rise Lubrication of Nanowire Array

Hong-huy Tran, Youngjin Kim, Céline TERNON, Michel Langlet, David Riassetto, Daeyeon Lee

► **To cite this version:**

Hong-huy Tran, Youngjin Kim, Céline TERNON, Michel Langlet, David Riassetto, et al.. Lubricant Depletion-Resistant Slippery Liquid-Infused Porous Surfaces via Capillary Rise Lubrication of Nanowire Array. *Advanced Materials Interfaces*, 2021, 8 (7), pp.2002058. 10.1002/admi.202002058 . hal-03215343

**HAL Id: hal-03215343**

**<https://hal.science/hal-03215343>**

Submitted on 9 Nov 2021

**HAL** is a multi-disciplinary open access archive for the deposit and dissemination of scientific research documents, whether they are published or not. The documents may come from teaching and research institutions in France or abroad, or from public or private research centers.

L'archive ouverte pluridisciplinaire **HAL**, est destinée au dépôt et à la diffusion de documents scientifiques de niveau recherche, publiés ou non, émanant des établissements d'enseignement et de recherche français ou étrangers, des laboratoires publics ou privés.

**Lubricant Depletion-Resistant Slippery Liquid-Infused Porous Surfaces via Capillary Rise Lubrication of Nanowire Array**

*Hong Huy Tran, Youngjin Kim, Céline Ternon, Michel Langlet, David Riassetto,\* and Daeyeon Lee\**

Hong Huy Tran, Dr. Youngjin Kim, Prof. Céline Ternon, Dr. Michel Langlet, Prof. David Riassetto  
Univ. Grenoble Alpes, CNRS, Grenoble INP (Institute of Engineering Univ. Grenoble Alpes),  
LMGP, 38000 Grenoble, France  
E-mail: [david.riassetto@grenoble-inp.fr](mailto:david.riassetto@grenoble-inp.fr)

Prof. Daeyeon Lee  
Department of Chemical and Biomolecular Engineering, University of Pennsylvania,  
Philadelphia, Pennsylvania 19104, United States  
E-mail: [daeyeon@seas.upenn.edu](mailto:daeyeon@seas.upenn.edu)

Keywords: liquid-infused surfaces, lubricant depletion, wetting ridge, ZnO nanowire arrays, capillarity

Despite their promise in diverse applications, lubricant depletion over time presents an important challenge for slippery lubricant-infused porous surfaces (SLIPS). The main source of lubricant depletion is the growth of a wetting ridge around a foreign liquid's droplet that removes the infused lubricant from the porous surface when the droplet slides off. Herein, we describe the fabrication of liquid-infused ZnO nanowire array surfaces by capillary rise lubrication and the effect of array morphology on suppressing wetting ridge formation. The orientation of nanowires strongly affects lubricant infiltration and the stability of SLIPS properties. The infiltrated lubricant in random ZnO nanowire arrays does not form a visible wetting ridge around a water droplet because of the strong capillarity that retains the lubricant confined in the nanoporous structure. The lack of wetting ridge gives rise to a stable SLIPS that exhibits self-recovery of the infused lubricant. Such a structure retains lubricant under a strong centrifugal force, showing high stability. Our study provides a straightforward, robust, and potentially scalable approach for making stable SLIPS that suppresses lubricant depletion by taking advantage of the unique morphology of the random nanowire arrays and capillary rise lubrication.

## 1. Introduction

Slippery lubricant-infused porous surfaces (SLIPS) show remarkable repellency against liquids, making them useful in diverse applications ranging from self-cleaning to water harvesting to anti-icing and anti-fouling.<sup>[1]</sup> The physical origin of the liquid repellency of SLIPS comes from a lubricant film within and above the surface of the porous template.<sup>[2]</sup> However, the lubricant film can be lost because of lubricant evaporation, shear force induced lubricant loss, and movement of liquid droplets on the infused surface.<sup>[3]</sup>

The depletion of lubricant in SLIPS presents a key barrier to the widespread adoption of this powerful approach. The formation of wetting ridges emerges as the primary source of lubricant depletion because of the interaction between a water droplet and the lubricant film.<sup>[4]</sup> This interaction induces the rising of a thin lubricant film around the water droplet or even to form a lubricant film that entirely covers the water droplet.<sup>[3c, 4a, 5]</sup> These wetting ridges degrade the performance of lubricant film over time when the water droplet slides off the surface, resulting in permanent loss of the lubricant.<sup>[4a]</sup> Furthermore, the removed lubricant presents a potential source of contamination in water harvesting applications.<sup>[6]</sup> It is thus critical to minimize or prevent the formation of wetting ridges, leading to stable SLIPS.

Despite its importance, suppression of wetting ridge on SLIPS has not been extensively addressed.<sup>[7]</sup> On the one hand, studies on SLIPS focus either on introducing new template/lubricant systems or exploring potential applications.<sup>[8]</sup> On the other hand, some studies reported the effect of viscosity and thickness of lubricant film on the SLIPS properties.<sup>[9]</sup> By carefully removing excess lubricant on a rough surface **by rotating the infused surface for a specific time to reach the desired thickness of lubricant, stable SLIPS** have been produced.<sup>[10]</sup> However, current coating approaches fail to produce such a stable infused configuration without time-consuming optimization steps **in which high shear force, causing the loss of repellency properties, is used.**

In this work, we describe a robust method for fabricating stable SLIPS via capillary rise infiltration (CaRI) of silicone oil into interstitial nanovoids of ZnO nanowire arrays. We hypothesize that the appearance of the wetting ridge and the subsequent loss of lubricant from SLIPS can be suppressed by eliminating extra lubricant outside the pores of the porous surface. To create such a structure, we infuse and confine silicone oil within the nanostructure of ZnO nanowire arrays via capillary forces. The silicone oil that resides in the interstitial pores between randomly aligned high aspect ratio ZnO nanowires can remarkably suppress the wetting ridge's growth. These structures also show excellent retention of silicone oil against moving water droplets and shear force, leading to highly stable SLIPS. Capillary rise lubrication enables eliminating excess lubricant without any delicate optimization steps, making it a potentially scalable manufacturing approach.

## **2. Results and Discussion**

### **2.1. Silicone oil-infused ZnO nanowire (NW) arrays via capillary rise lubrication**

Capillarity at the nanoscale is a powerful force that enables the spontaneous transport of liquid into small pores.<sup>[11]</sup> Here, we induce infusion and retention of silicone oil in the nanostructure of ZnO NW arrays via capillarity to produce stable SLIPS. The advantage of ZnO NW arrays is that the porous structure's morphology can be varied by changing the orientation of NWs. For example, ZnO NW arrays with vertical or random alignments can be produced. These different alignments likely result in interstitial pores of different shapes and sizes. Here, we study how the orientation of ZnO NWs affects the silicone oil infiltration and the stability of infiltrated surfaces against lubricant depletion.

ZnO NW arrays are grown on pre-seeded silicon wafer substrates via a chemical bath deposition method.<sup>[12]</sup> The orientation of NWs is controlled by changing the number of the seed layer and the heat treatment step before immersion in the growth solution.<sup>[12a]</sup> We study three types of ZnO NW arrays having different orientations: vertical, tilted, and random

geometry. The morphology of the three types of ZnO NW arrays before the infiltration of silicone oil is observed through scanning electron microscopy (SEM). The top-view SEM images (**Figure 1a-c**) indicate the presence of NW arrays with different orientation angles. Cross-section SEM images (Figure 1d and e) show that the vertical and tilted NW arrays have orientation angles of  $3.7^\circ \pm 3.15^\circ$  and  $19.3^\circ \pm 9.3^\circ$ , respectively (Figure S1, Supporting Information (SI), for statistical details). When NWs are grown with a high aspect ratio (i.e., the ratio between the length and diameter), they undergo aggregation to form bundles upon drying. Because of this aggregated morphology, we classify this structure as the random NW array (Figure 1f and Figure S2). These three types of ZnO NW arrays will be hereafter

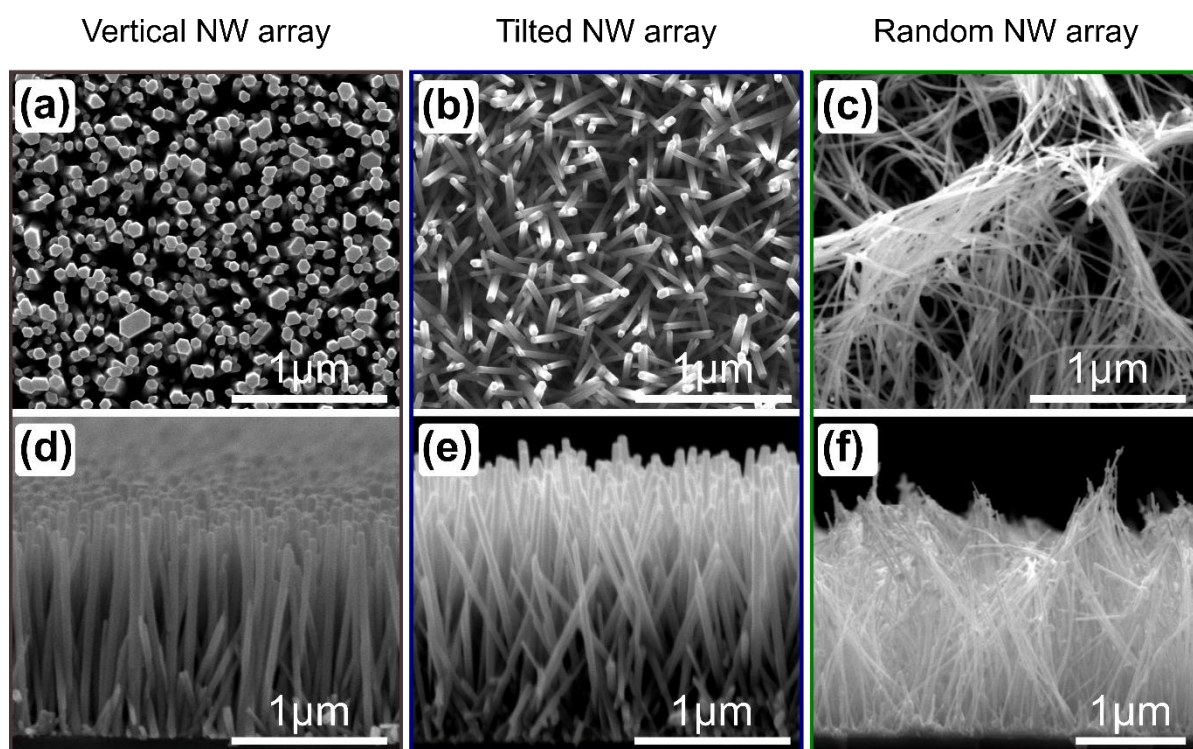


**Figure 1.** (a-c) Top-view and (d-f) cross-section SEM images of the ZnO NW arrays with three types of orientation.

referred to as vertical NW array, tilted NW array, and random NW array, respectively.

To prepare lubricant-infused surfaces, we induce wicking of silicone oil into the interstitial nanogaps of ZnO NW arrays (**Figure 2a**). We hypothesize that this approach will confine

silicone oil within the interstitial voids between NWs and eliminate extra lubricant surfaces.

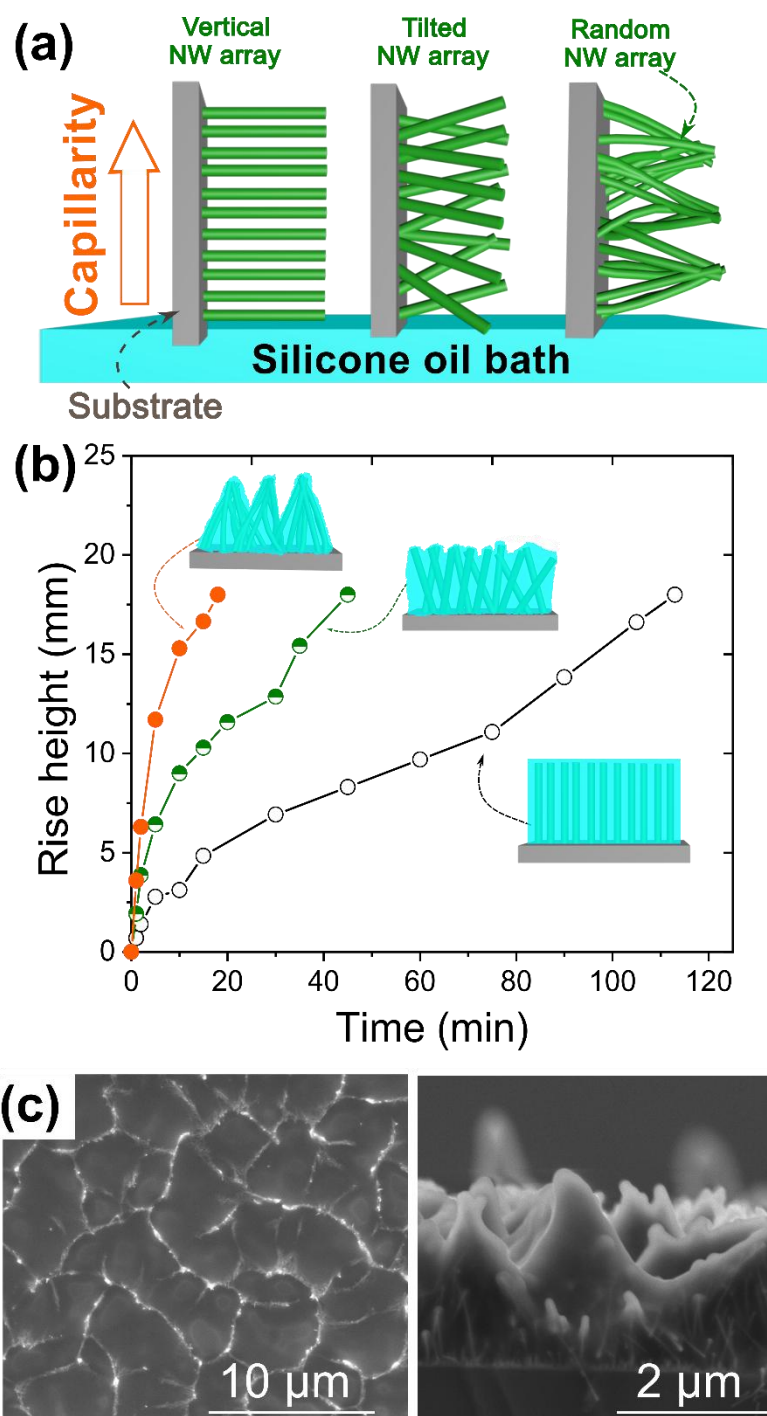


**Figure 2.** (a) Schematic illustration of the capillary rise infiltration (CaRI) lubrication of ZnO NW arrays with silicone oil. For clarity, objectives are not drawn to scale. (b) Wicking rate of silicone oil in the structure of ZnO NW arrays with three types of orientation. (c) SEM images of the random ZnO NW array upon lubrication.

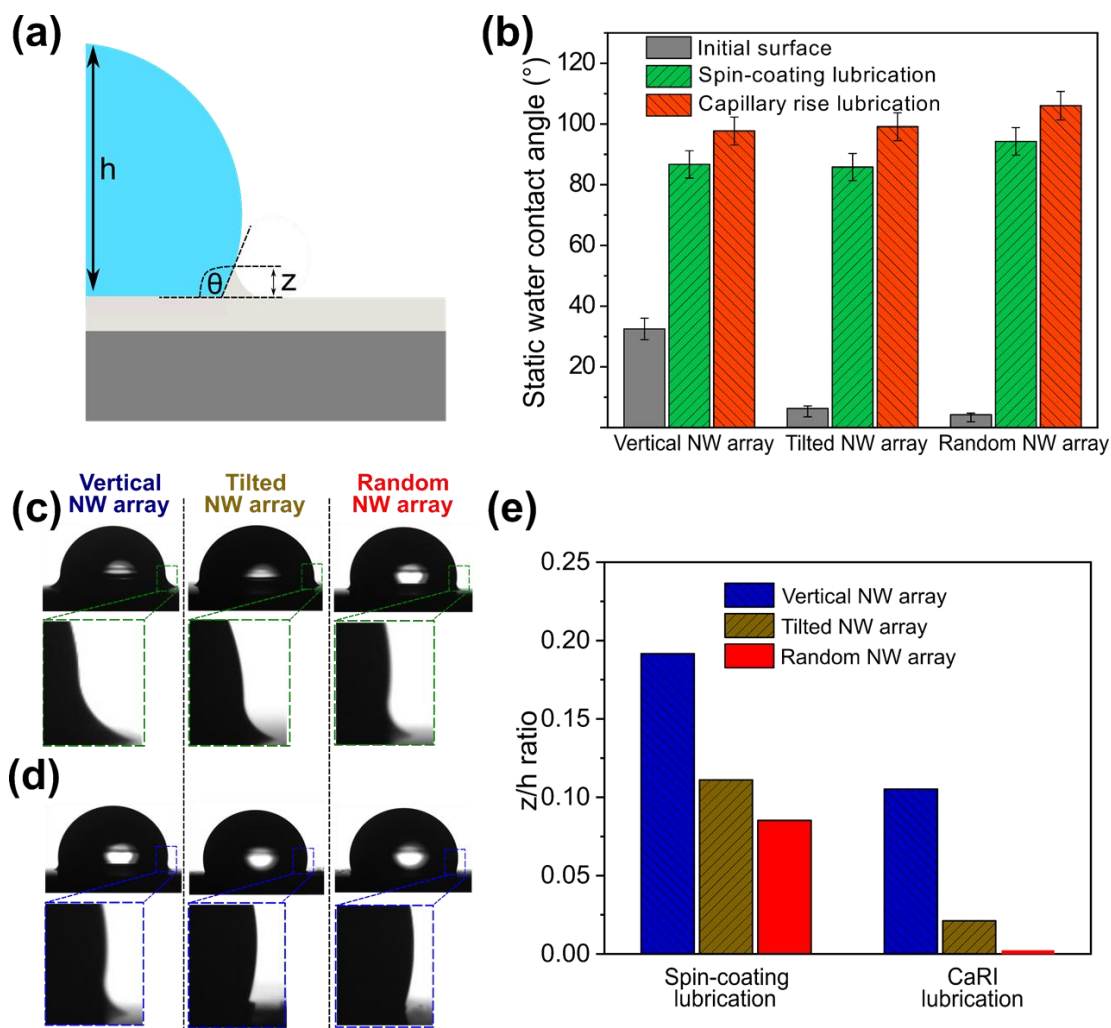
Three types of NW arrays show a clear difference in the silicone oil rising rates (Figure 2b).

The vertical ZnO NW array shows the slowest rate of silicone oil infiltration requiring 115 min to rise 1.8 cm. In comparison, the tilted ZnO NW array takes about 45 min to rise to the same height. For the random ZnO NW array, composed of long and dense NWs, only about 18 min is needed to rise to the same height. As the liquid and material are the same between the three samples, we may consider that the dynamic viscosity, surface tension, and contact angle are constant for all the samples. Based on these assumptions and the dependence of wicking rate on the pore size,<sup>[11f, 13]</sup> these observations suggest that the capillary pressure in the random NW array sample is the largest among the three types of NW arrays. The random NW array likely presents a nanoscale porous structure within aggregated NW bundles, possibly explaining the robust wicking of this sample (Figure 1c, f, and Figure S2). The same wicking trend is also observed in our wicking experiments with water; the random NW array has the most rapid wicking rate among the three structures (Figure S3). Upon infiltration, the random NW array presents a rough lubricated structure where the silicone oil is confined within the NW bundles. No visible silicone oil in the valleys between the aggregated NWs bundles is observed, likely because the capillary force is considerably strong at the nanoscale (Figure 2c).

## 2.2. Wetting properties of the silicone oil-infused ZnO NW array surfaces

To understand the effect of extra lubricant on the wetting properties (i.e., the lubricant that is not confined in the interstices between NWs), we compare NW arrays lubricated by our capillary rise infiltration (CaRI) method with those lubricated using a standard top-down approach, i.e., lubrication by spin-coating of silicone oil directly onto the surface. The illustration of a wetting ridge surrounding a water droplet on a lubricant-infused surface and the definition of the apparent contact angle is presented in **Figure 3a**. Water droplet contact angles on ZnO NW arrays spin-coated lubricant are between 80° and 90°. Water contact angles on the CaRI-lubricated NW arrays are larger than the corresponding values on spin-

coated samples (Figure 3b). The random array has the highest contact angle of the three, likely because of its high surface roughness (Figure 1c, f, and Figure S2). Water droplets have prominent wetting ridges on all these spin-coated surfaces because of the rise of the lubricant film around the water droplet (Figure 3c, see the inset zoomed pictures for clarity). The



appearance of wetting ridge suggests that a thin layer of extra lubricant (i.e., lubricant that is not confined in the interstitial void between NWs) exists above the height of the NWs. These wetting ridges are identified as the main source of lubricant depletion on liquid-infused surfaces.<sup>[4a, 5a, 14]</sup>

**Figure 3.** (a) A schematic illustration of a water droplet on a lubricant-infused surface, showing a wetting ridge and definition of apparent contact angle. (b) Static water contact angle on ZnO NW arrays before and after infusion of silicone oil via spin coating and CaRI.

(c) Micrographs of water droplets on the surface of ZnO NW arrays after infiltration of silicone oil via spin coating. (d) Micrographs of water droplets on the surface of ZnO NW arrays after infusion of silicone oil by CaRI. (e) Comparative analysis of  $z/h$  ratio of a water droplet on lubricant-infused surfaces using spin-coating and CaRI.  $h$  represents the water droplet's height after sitting on the lubricant-infused surface, and  $z$  represents the height of the wetting ridge.

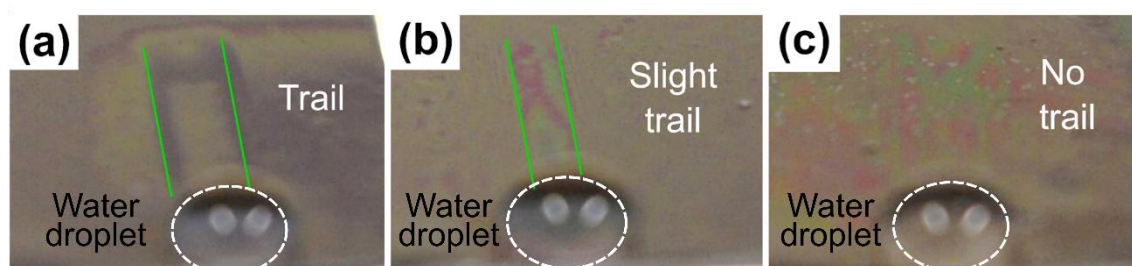
Remarkably, we observe a transition in the shape of the wetting ridge on CaRI-lubricated NW arrays as the orientation of the NWs is changed (see dashed blue insets in Figure 3d for clarity). A wetting ridge is observed around the water droplet on the vertical NW array (Figure 3d); however, the wetting ridge's size is considerably reduced compared to the one observed on spin-coated samples (Figure 3c). The formation of wetting ridge is considerably suppressed for the tilted NW array and not visible for the random NW array (Figure 3d).

For quantitative analysis, we evaluate the CaRI lubrication method's effectiveness in suppressing the growth of wetting ridge by calculating the ratio of lubricant ridge height ( $z$ ) to the water droplet height ( $h$ ), see Figure 3e. The  $z/h$  ratios in NW arrays spin-coated lubricant show high values because of a wetting ridge's prominent presence. However, the  $z/h$  ratio is lower for the tilted NW array and the random NW array than that of the vertical NW array (Figure 3e). Using the CaRI lubrication approach, the  $z/h$  ratio is remarkably decreased for the vertical NW array and the tilted NW array compared to those observed on spin-coated samples. On the lubricated random NW array surface, the wetting ridge is no longer visible, and it is not possible to calculate the  $z/h$  ratio. These results are consistent with the rates of capillary rise (Figure 2b). Because of the nanoscale porous structure-induced high capillary pressure posed by tilted and random NW arrays, the infused lubricant stays trapped in the interstices among the NWs and does not form wetting ridges. Also, as NW arrays' morphology varies from vertical to tilted and to random alignments, NW arrays' structure

provides a more tortuous path for the lubricant to escape. For instance, the vertical NW array shows a uniform channel-like path (Figure 1a), providing a direct path for lubricant to go from the bottom surface to the top. The tilted NW array provides a more tortuous path via the collision of NWs, but there are remaining open paths for the lubricant from the bottom to reach the top surface (Figure 1b). Of interest is the random NW array's unique morphology, consisting of NW bundles, likely provides a highly tortuous path and thus effectively confines lubricant within the aggregated NW bundles. Thus, the combination of the high capillary pressure and extremely tortuous path likely play important roles in resisting the growth of wetting ridge, potentially addressing the problem of lubricant depletion.

### 2.3. Stability of silicone oil-infused ZnO NW array surfaces under dynamic conditions

As described above, moving and shedding water droplets on lubricant-infused surfaces lead to lubricant loss if the water droplets are surrounded by wetting ridges. Thus, it is critical to make a stable lubricant-infused surface showing liquid repellency under dynamic (i.e., water-shedding) conditions. To gain more insights into the wetting ridge's effect on the lubricant depletion, we perform various experiments to observe NW morphology's impact on lubricant-infused NW arrays' stability. We first observe the traces left by water droplets sliding on lubricant-infused ZnO NW arrays. A trail is left by a sliding droplet on the vertical NW array (Figure 4a), dragging lubricant with it, presumably because of the wetting ridge's presence. The tilted NW array with lubricant also shows a slight trail left by a moving droplet as shown in Figure 4b. In contrast, no visible track is seen on the lubricated random NW array surface after a droplet slid down the surface (Figure 4c). This observation agrees with the results shown in Figure 3; surfaces that suppress the ridge formation reduce lubricant loss from the



surface.

**Figure 4.** Digital photographs of trails left by sliding water droplets on silicone oil-infused (a) vertical NW array, (b) tilted NW array, and (c) random NW array samples. The diameter of the water droplets is approximately 1 mm.

Loss of lubricant from SLIPS can also be induced by a mechanical force such as shear or centrifugal.<sup>[3b]</sup> Few robust strategies against mechanical force-driven lubricant depletion have been presented.<sup>[15]</sup> We compare the stability of SLIPS properties against mechanical force-induced lubricant depletion by applying a strong centrifugal force using a spin coater for 180 s at a speed of 4500 rpm and measuring the sliding velocity of a water droplet on the 7°-inclined surface (**Figure 5**). Previous studies have shown that the velocity of a water droplet sliding on lubricant-infused surfaces is proportional to the lubricant film's thickness and conformality.<sup>[16]</sup> Consistent with this observation, a water droplet on the lubricated vertical NW array before applying centrifugal force has the fastest sliding velocity among the three NW arrays. The difference in the thickness of lubricant on the lubricated NW arrays' surface can also be inferred from the difference in the moving trail (Figure 4).

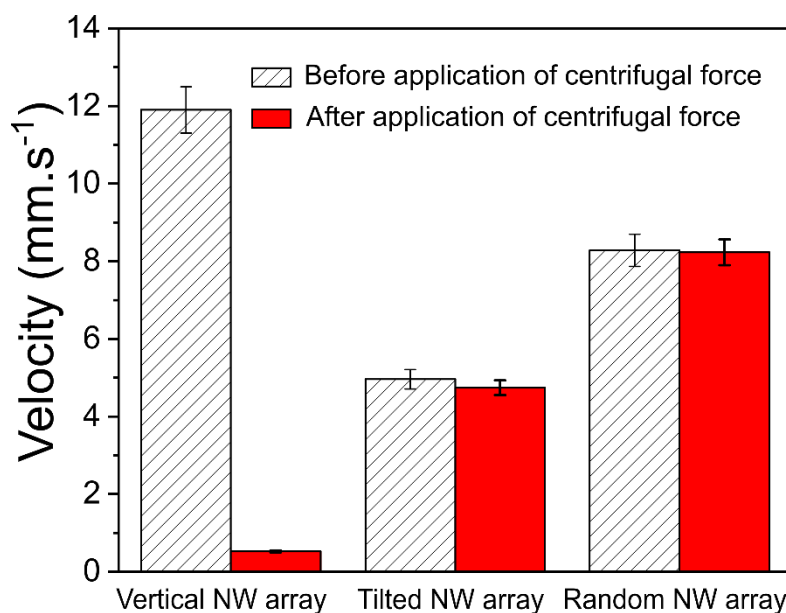
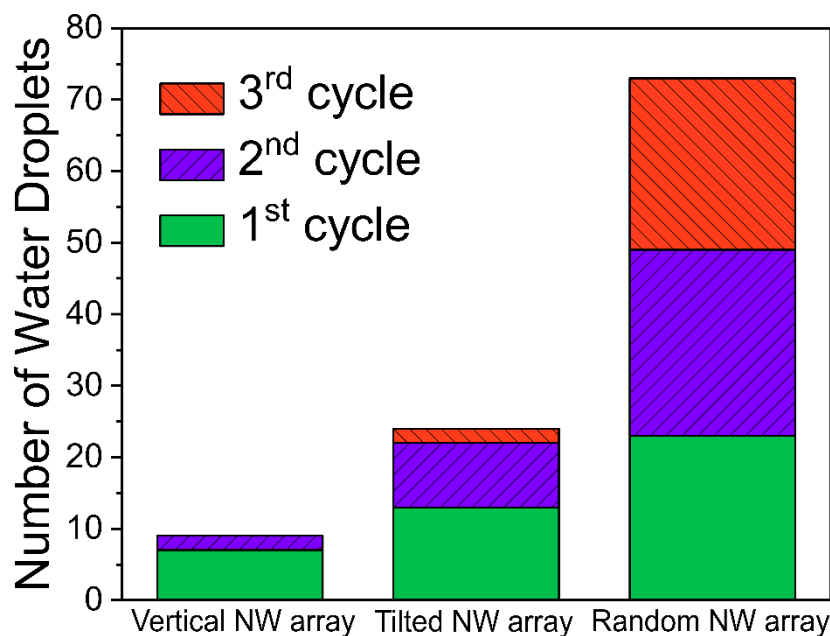


**Figure 5.** The sliding velocity of water droplets on the 7°-inclined surface before and after applying a high-speed spinning test. The stability of the infused ZnO NW arrays against centrifugal force-induced failure is performed using a spin coater, rotating at a spin speed of 4500 rpm for 180 s.

After applying a strong centrifugal force, we observe a considerable decrease in the sliding speed of a water droplet (~23-fold decrease) on the vertical NW array. Remarkably, the lubricated random NW array does not show any reduction in the sliding velocity of a water droplet after it has been subjected to the high centrifugal force. In contrast, a small decrease in the sliding speed is observed for the tilted array. These results suggest that the orientation of NW arrays indeed plays an important role in the retention of lubricant against a mechanical force, likely by providing nanoscale pores and tortuous paths for lubricant depletion.

We also study the lubricant retention using a water droplet impact experiment in which water drops are dripped onto the surface of each sample (tilt angle of 7°) from a height of 2 cm. Each water droplet is approximately 50  $\mu$ L in volume, and water droplets are dripped at the frequency of roughly one droplet/sec. The number of water droplets striking and sliding off the surface of lubricant-infused NW arrays are counted until a water droplet stops sliding.

Results indicate that the lubricant-infused random NW array can shed at least 23 water droplets from the same area (**Figure 6**). In contrast, lubricant-infused vertical and tilted NW



arrays lose their liquid repellency after shedding only 6 and 13 water droplets, respectively.

**Figure 6.** Water droplet impact test, which shows the number of water droplets that shed from lubricated surfaces after one cycle (green-blank), two cycles (purple with right-to-left lines pattern), and three cycles (red with left-to-right lines pattern).

To study the self-recovery of SLIPS properties, we leave our samples five minutes in an ambient condition after they lose their repellency due to repeated droplet impact and re-perform the water impact test by dropping water droplets in the same area. Just one or two droplets can slide on the surface of the vertical NW array during the second round of the water impact experiment. After the second round, this array completely loses its ability to shed water droplets. The lubricant-infused tilted array shows some recovery of the SLIPS property: 9 and 2 water droplets shed off in the second and third rounds of water impact tests, respectively. Notably, the lubricant-infused random NW array retains its water repellency

without showing any reduction in the number of water droplets that can be shed after three cycles (Figure 6). Thus, the random NW array can recover its repellency rapidly without any external intervention after just five minutes.

### 3. Conclusion

In conclusion, we have described a robust approach for fabricating lubricant depletion-resistant slippery liquid-infused porous surfaces by inducing infiltration of silicone oil into interstitial nanogaps of ZnO nanowire (NW) arrays via capillary rise infiltration. By controlling the orientation of ZnO NW arrays, we show that random orientation and aggregation of long NWs are critical in suppressing the appearance of the wetting ridge. Such morphology likely gives nanoscale pores that provide a large capillary pressure and a highly tortuous path, leading to excellent retention of silicone oil against moving water droplets and external forces. Our study provides a robust approach for making stable, and self-healing SLIPS surfaces by circumventing the problem of lubricant depletion. While our work convincingly showed the importance of providing high capillary pressure to suppress lubricant depletion, the best performing surface also has a unique morphology compared to typical SLIPS surfaces; that is, the surface topography after lubricant infusion retains micro-scale roughness. The role of such a roughness has not been extensively studied for SLIPS surfaces and warrants future investigation.

### 4. Experimental Section

*Preparation of ZnO NW arrays:* ZnO NW arrays with three types of orientation are hydrothermally grown onto pre-seeded silicon substrates (3 cm × 3 cm) using a sol-gel process.<sup>[12]</sup> The substrates are cleaned with ethanol and treated with oxygen plasma to promote the adhesion of the ZnO seed layer. The orientation of ZnO NWs is controlled by changing the number of seed layers and the seed layer's heat treatment before the hydrothermal process.<sup>[12a]</sup> For depositing a ZnO seed layer, 300 μL of 0.37 M zinc acetate dehydrate sol is spin-coated on a cleaned silicon wafer substrate. Deposition is performed at a

rotation speed of 3000 rpm for 10 s, followed by 30 s of solvent evaporation. To prepare a vertical ZnO NW array, two seed layers are deposited on the silicon wafer, whereas one seed layer is deposited to make a tilted ZnO NW array. The ZnO seed layer-coated substrates are placed in an oven at 540 °C for 1 h to promote the crystallization of ZnO. The seeded substrate is held using a Teflon holder with a 45° tilt angle and immersed in a 200 mL mixture of hexamethylenetetramine and zinc nitrate hexahydrate (the concentration of 25 mM for both solutions) that is preheated at 90 °C on a hot plate. The time for growing ZnO NW arrays is 2 h. To prepare random ZnO NW arrays, the one seed layer-coated substrate is treated with oxygen plasma for 2 min and preheated at 135 °C for 15 min before the hydrothermal step. The growth solution is prepared by mixing 400 µL of zinc nitrate hexahydrate in 199.2 mL of deionized water, followed by heating the solution to 90 °C. At 90 °C, 400 µL of hexamethylenetetramine is added; the mixture is then stirred for 2 min. The preheated seed layer is then immersed in the growth solution for 4 h to produce high aspect ratio random NW arrays. A statistical analysis of ZnO NW arrays' geometry is provided in the SI (Figure S1). Silicone oil with a viscosity of 20 cSt (25 °C) is purchased from Sigma Aldrich. The surface energy of the silicone oil is 24 mJ.m<sup>-2</sup> at 20 °C. Deionized water is used in all experiments.

*Preparation of silicone oil-infused ZnO NW arrays via capillary rise infiltration:* Silicon substrates with ZnO NW arrays on the surface are thermally treated in an oven at 540 °C for 30 min to remove organic residues and water vapor before the wicking experiment. The substrates with ZnO NWs arrays are cut into 2 cm × 2 cm pieces and are held vertically in a silicone oil bath. The wicking dynamics are captured using a digital camera. In our experiments, we denote the  $t = 0$  is when the sample surface touches silicone oil, and silicone oil starts to infuse vertically from the initial wicking front position. Surface modification of ZnO NW arrays is not necessary to induce wicking of silicone oil, likely due to their high surface energy. We also prepare silicone oil-infused ZnO NW arrays by a general procedure

in which silicone oil is coated onto the surface of ZnO NW arrays using a spin coater (1000 rpm for 60 s).<sup>[2, 10b]</sup> After the spin-coating step, the surface of ZnO NW arrays is infused and covered by a smooth silicone oil layer.

*Characterization:* Scanning electron microscopy (SEM) images are taken on a FEI QUANTA 250 to observe the morphology of ZnO NW arrays. SEM images are captured at an accelerating voltage of 5 kV and a working distance of 10 mm. SEM images of silicone oil-lubricated samples are captured in a low-vacuum mode; liquid nitrogen can be used to cool down and stabilize infused samples. The sessile drop method is used for observing the apparent water contact angle values and the shape of water droplets on the surface after the infusion of silicone oil using a Krüss, DSA10-MK2 goniometer connected with a video camera at room temperature. Five water droplets of 5  $\mu$ L volume are placed on different points of a horizontally mounted sample surface using a microsyringe.

*Trail detection from moving water droplets:* The samples are tilted at an angle of 7°; a water droplet (~50  $\mu$ L in volume) is dripped from a syringe held 2 cm above the sample surface. The water droplet is dripped from the syringe tip and subsequently slides on the infused surfaces. We observe these moving droplets using a digital camera.

*Water droplet impact test:* Silicone oil-infused surfaces are placed with a tilt angle of 7° under a water container. Water is dripped dropwise from the container tip and contacts the silicone oil-infused surfaces, subsequently sliding off the surface. We count the number of water droplets that move and shed from the surface until a water droplet stops moving on the surface.

*Centrifugal force-resistance test via high-speed spinning:* The stability of the as-prepared slippery silicone oil-infused ZnO NW arrays against centrifugal force-induced failure is studied using a spin coater. The silicone oil-infused surfaces are rotated at a spin speed of 4500 rpm for 180 s and then examined their sliding behavior. The velocity of a water droplet sliding on the surface before and after the high-speed spinning treatment is measured on a

sample with a tilt angle of 7°; water droplets are dripped from a syringe held 2 cm above the sample surface.

### Supporting Information

Supporting Information is available from the Wiley Online Library or from the author.

### Conflict of Interest

There are no conflicts to declare.

### Acknowledgements

The authors acknowledge the Chair of Excellence Program's support from the Nanosciences Foundation (Université Grenoble Alpes Foundation). This work was also supported by NSF PIRE grant 1545884 and ANR grant ANR-15-PIRE-0001-02. Hong Huy Tran thanks the IDEX for funding the travel grant. The authors thank Dr. Cyril Picard, Dr. Marianne Weidenhaupt, Dr. Tim Murdoch, Gélard Isabelle, R. Bharath Venkatesh, and Paradorn Rummaneethorn for helpful suggestions and technical help.

Received: ((will be filled in by the editorial staff))

Revised: ((will be filled in by the editorial staff))

Published online: ((will be filled in by the editorial staff))

### References

- [1] a) T. S. Wong, S. H. Kang, S. K. Tang, E. J. Smythe, B. D. Hatton, A. Grinthal, J. Aizenberg, *Nature* **2011**, 477, 443; b) X. Dai, N. Sun, S. O. Nielsen, B. B. Stogin, J. Wang, S. Yang, T. S. Wong, *Sci Adv* **2018**, 4, eaaq0919; c) S. Anand, A. T. Paxson, R. Dhiman, J. D. Smith, K. K. Varanasi, *ACS Nano* **2012**, 6, 10122; d) P. Kim, T. S. Wong, J. Alvarenga, M. J. Kreder, W. E. Adorno-Martinez, J. Aizenberg, *ACS Nano* **2012**, 6, 6569; e) D. C. Leslie, A. Waterhouse, J. B. Berthet, T. M. Valentin, A. L. Watters, A. Jain, P. Kim, B. D. Hatton, A. Nedder, K. Donovan, E. H. Super, C. Howell, C. P. Johnson, T. L. Vu, D. E. Bolgen, S. Rifai, A. R. Hansen, M. Aizenberg, M. Super, J. Aizenberg, D. E. Ingber, *Nat Biotechnol* **2014**, 32, 1134; f) S. Amini, S. Kolle, L. Petrone, O. Ahanotu, S. Sunny, C. N. Sutanto, S. Hoon, L. Cohen, J. C. Weaver, J. Aizenberg, N. Vogel, A. Miserez, *Science* **2017**, 357, 668; g) C. Wang, Y. Yan, D. Du, X. Xiong, Y. Ma, *ACS Appl Mater Interfaces* **2020**, 12, 29767; h) D. Quéré, *Reports on Progress in Physics* **2005**, 68, 2495; i) K. C. Park, P. Kim, A. Grinthal, N. He, D. Fox, J. C. Weaver, J. Aizenberg, *Nature* **2016**, 531, 78; j) L. Chen,

- S. Park, J. Yoo, H. Hwang, H. Kim, J. Lee, J. Hong, S. Wooh, *Advanced Materials Interfaces* **2020**, 7; k) Y. Cao, S. Jana, X. Tan, L. Bowen, Y. Zhu, J. Dawson, R. Han, J. Exton, H. Liu, G. McHale, N. S. Jakubovics, J. Chen, *Langmuir* **2020**, 36, 13396.
- [2] J. Wang, L. Wang, N. Sun, R. Tierney, H. Li, M. Corsetti, L. Williams, P. K. Wong, T.-S. Wong, *Nature Sustainability* **2019**, 2, 1097.
- [3] a) J. H. Guan, G. G. Wells, B. Xu, G. McHale, D. Wood, J. Martin, S. Stuart-Cole, *Langmuir* **2015**, 31, 11781; b) J. S. Wexler, I. Jacobi, H. A. Stone, *Phys Rev Lett* **2015**, 114, 168301; c) D. Daniel, J. V. I. Timonen, R. Li, S. J. Velling, J. Aizenberg, *Nature Physics* **2017**, 13, 1020.
- [4] a) M. J. Kreder, D. Daniel, A. Tetreault, Z. Cao, B. Lemaire, J. V. I. Timonen, J. Aizenberg, *Physical Review X* **2018**, 8; b) S. J. Park, B. M. Weon, J. S. Lee, J. Lee, J. Kim, J. H. Je, *Nat Commun* **2014**, 5, 4369.
- [5] a) F. Schellenberger, J. Xie, N. Encinas, A. Hardy, M. Klapper, P. Papadopoulos, H. J. Butt, D. Vollmer, *Soft Matter* **2015**, 11, 7617; b) A. A. Günay, S. Sett, Q. Ge, T. Zhang, N. Miljkovic, *Advanced Materials Interfaces* **2020**, 7.
- [6] S. Adera, J. Alvarenga, A. V. Shneidman, C. T. Zhang, A. Davitt, J. Aizenberg, *ACS Nano* **2020**, 14, 8024.
- [7] X. Chen, G. Wen, Z. Guo, *Materials Horizons* **2020**, DOI: 10.1039/d0mh00088d.
- [8] a) X. Jing, Z. Guo, *ACS Appl Mater Interfaces* **2019**, 11, 35949; b) Z. Wang, Z. Guo, *Nanoscale* **2018**, 10, 19879; c) N. R. Geraldi, J. H. Guan, L. E. Dodd, P. Maiello, B. B. Xu, D. Wood, M. I. Newton, G. G. Wells, G. McHale, *Sci Rep* **2019**, 9, 13280; d) K. Manabe, M. Nakano, Y. Hibi, K. Miyake, *Advanced Materials Interfaces* **2020**, 7, 1901818.
- [9] a) Z. Wang, L. Heng, L. Jiang, *Journal of Materials Chemistry A* **2018**, 6, 3414; b) M. Muschi, B. Brudieu, J. Teisseire, A. Sauret, *Soft Matter* **2018**, 14, 1100; c) C. Lee, H. Kim, Y. Nam, *Langmuir* **2014**, 30, 8400; d) J. H. Kim, J. P. Rothstein, *Langmuir* **2016**,

- 32, 10166; e) Y. Liu, J. S. Wexler, C. Schönecker, H. A. Stone, *Physical Review Fluids* **2016**, 1.
- [10] a) S. Peppou-Chapman, C. Neto, *ACS Appl Mater Interfaces* **2018**, 10, 33669; b) X. Dai, B. B. Stogin, S. Yang, T. S. Wong, *ACS Nano* **2015**, 9, 9260; c) C. S. Ware, T. Smith-Palmer, S. Peppou-Chapman, L. R. J. Scarratt, E. M. Humphries, D. Balzer, C. Neto, *ACS Applied Materials & Interfaces* **2018**, 10, 4173.
- [11] a) J. Lee, Y. Suh, P. P. Dubey, M. T. Barako, Y. Won, *ACS Appl Mater Interfaces* **2019**, 11, 1546; b) Z. Wang, J. Zhao, A. Bagal, E. C. Dandley, C. J. Oldham, T. Fang, G. N. Parsons, C. H. Chang, *Langmuir* **2016**, 32, 8029; c) H. H. Tran, R. B. Venkatesh, Y. Kim, D. Lee, D. Riassetto, *Nanoscale* **2019**, 11, 22099; d) R. B. Venkatesh, S. H. Han, D. Lee, *Nanoscale Horizons* **2019**, 4, 933; e) N. Manohar, K. J. Stebe, D. Lee, *Macromolecules* **2020**, 53, 6740; f) Y. Yao, H. J. Butt, G. Floudas, J. Zhou, M. Doi, *Macromol Rapid Commun* **2018**, 39, e1800087.
- [12] a) T. Demes, C. Ternon, D. Riassetto, H. Roussel, L. Rapenne, I. Gélard, C. Jimenez, V. Stambouli, M. Langlet, *Journal of Physics and Chemistry of Solids* **2016**, 95, 43; b) T. Demes, C. Ternon, F. Morisot, D. Riassetto, M. Legallais, H. Roussel, M. Langlet, *Applied Surface Science* **2017**, 410, 423.
- [13] X. Chen, J. Chen, X. Ouyang, Y. Song, R. Xu, P. Jiang, *Langmuir* **2017**, 33, 6701.
- [14] M. Tress, S. Karpitschka, P. Papadopoulos, J. H. Snoeijer, D. Vollmer, H. J. Butt, *Soft Matter* **2017**, 13, 3760.
- [15] a) P. Baumli, H. Teisala, H. Bauer, D. Garcia-Gonzalez, V. Damle, F. Geyer, M. D'Acunzi, A. Kaltbeitzel, H. J. Butt, D. Vollmer, *Adv Sci (Weinh)* **2019**, 6, 1900019; b) J. D. Smith, R. Dhiman, S. Anand, E. Reza-Garduno, R. E. Cohen, G. H. McKinley, K. K. Varanasi, *Soft Matter* **2013**, 9, 1772; c) I. Sotiri, A. Tajik, Y. Lai, C. T. Zhang, Y. Kovalenko, C. R. Nemr, H. Ledoux, J. Alvarenga, E. Johnson, H. S. Patanwala, J. V. I. Timonen, Y. Hu, J. Aizenberg, C. Howell, *Biointerphases* **2018**, 13, 06D401.

- [16] P. Kim, M. J. Kreder, J. Alvarenga, J. Aizenberg, *Nano Lett* **2013**, 13, 1793.

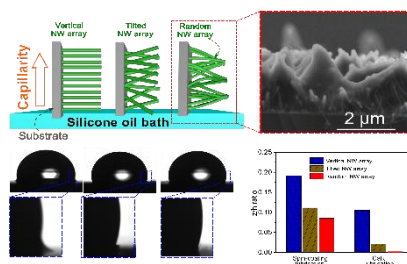
**Table of contents entry**

A robust method for producing stable slippery lubricant-infused porous surfaces (SLIPS) that resist lubricant depletion is described. The combination of the unique morphology provided by the random nanowire array and capillary rise lubrication gives a potentially scalable method to produce lubricant loss-resistant SLIPS.

Hong Huy Tran, Youngjin Kim, Céline Ternon, Michel Langlet, David Riassetto,\* and Daeyeon Lee\*

**Lubricant Depletion-Resistant Slippery Liquid-Infused Porous Surfaces via Capillary Rise Lubrication of Nanowire Array**

ToC figure (55 mm broad × 50 mm high)



## Supporting Information

**Lubricant Depletion-Resistant Slippery Liquid-Infused Porous Surfaces via Capillary Rise Lubrication of Nanowire Array**

*Hong Huy Tran, Youngjin Kim, Céline Ternon, Michel Langlet, David Riassetto,\* and Daeyeon Lee\**

**Table of content**

**Figure S1:** Statistical analysis of the orientation angle of ZnO NW arrays.

**Figure S2:** Additional SEM images of random ZnO NW array.

**Figure S3:** Shape of a water droplet on the initial surfaces of ZnO NW arrays.

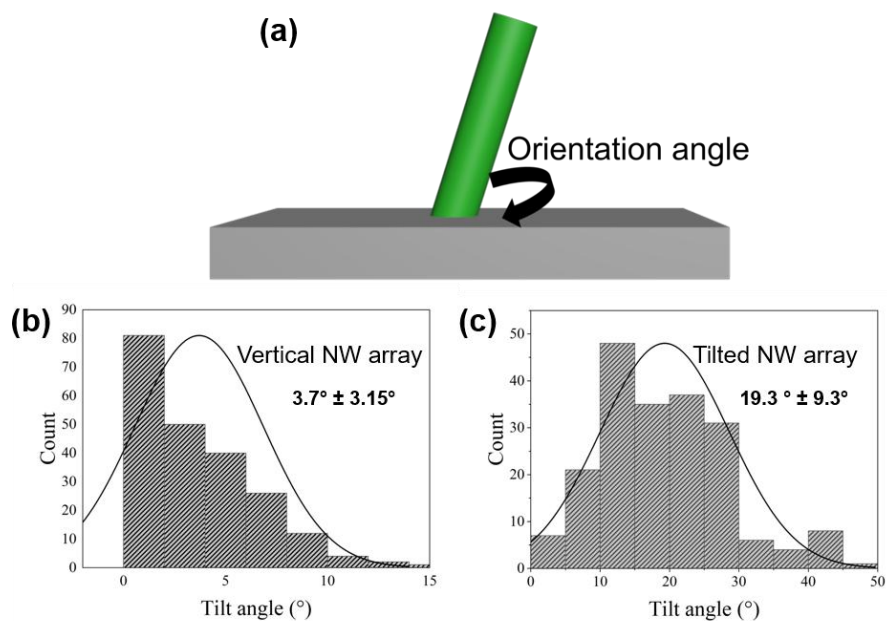


**Figure S1.** (a) Definition of the orientation angle of NWs. Statistical analysis of the orientation angle of ZnO NW arrays, including (b) vertical NW array and (c) tilted NW array. At least 250 NWs are analyzed. The error bar is calculated based on the standard deviation.

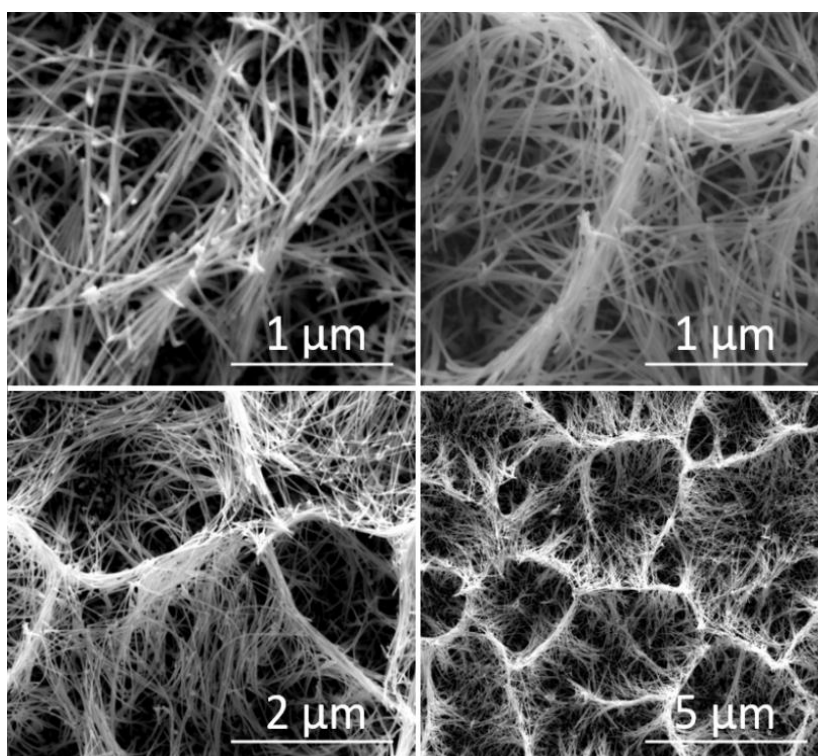


**Figure S2.** Additional SEM images of random ZnO NW array.

**Effect of pore size on capillary pressure**

$$\Delta P_{cap} = \frac{2\gamma \cos\theta}{R} \quad (1)$$

Theoretically, the capillary pressure ( $P_{cap}$ ) causes the rise of the liquid (that has a surface tension  $\gamma$ ) inside the capillary tube if the radius of the capillary tube ( $R$ ) is small enough such that the ( $P_{cap}$ ) is greater than the atmospheric pressure.  $\cos\theta$  represents the contact angle between the tube wall and the liquid; a contact angle less than  $90^\circ$  leads to the rising of the liquid inside the tube. From Equation 1, a smaller pore size generally leads to greater capillary pressure, inducing a faster wicking rate of liquid in comparison to a pore with a larger radius.<sup>[1]</sup>

**Surface wettability of the initial ZnO NW arrays**

The surface of the ZnO NW arrays with the three types of orientation are all inherently hydrophilic before the infiltration of silicone oil, as shown in Figure S3. Moreover, the water contact angle on the surface of the ZnO NW arrays decreases as the verticality decreases, which agrees well with the trends observed in the rates of silicone oil wicking (Figure 2). High capillary pressure present in the nanostructure of the randomly aligned NW array likely induces wicking-induced wetting of water, leading to such a low water contact angle.

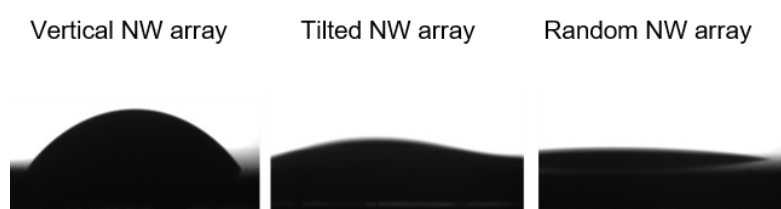


**Figure S3.** Shape of water droplet on the initial surface of ZnO NW arrays.

## References

- [1] a) Pierre-Gilles de Gennes, Françoise Brochard-Wyart; Quéré, D, *Capillarity and wetting phenomena: drops, bubbles, pearls, waves. Capillarity and wetting phenomena: drops, bubbles, pearls, waves*, Springer-Verlag, NY, **2013**. b) D. Bonn, , J. Eggers, J. Indekeu, J. Meunier, E. Rolley, *Rev. Mod. Phys.* **2013**, 81, 739.

